ORIGINAL ARTICLE

Assessment of Biocompatibility and Physical Properties of Ni–Ti–Zr–Nb Shape Memory Alloys

S. S. Abdullah[1,2] · E. Balci[1] · I. N. Qader[3] ·
F. Dagdelen[1]

Abstract Ti–Ni-based shape memory alloys (SMAs) are among the alloys used as biomaterials. The degree of biocompatibility can be improved by adding different biocompatible elements to these alloy families. In this study, the microstructure, phase transformation temperatures, and biocompatibility of Ti–Ni–Nb–Zr SMAs were investigated by scanning electron microscopy (SEM), energy dispersive X-ray spectroscopy (EDS), optical microscopy (OM), differential scanning calorimetry (DSC), and electrochemical potentiodynamic measurements, respectively. The arc melting method was used to manufacture alloys with nominal compositions of Ti–10Zr–(40-x) Ni–xNb ($x = 0$, 2 and 4 at.%). The phase transformation of B19′ ↔ B2 was observed in DSC results, which indicated that the alloys have shape memory behavior. Although martensite plates and dendritic structures are noticeable in OM images, XRD and SEM analyses revealed β-Nb, B19′, B2, and some precipitation phases. The corrosion resistance of the alloys was determined by potentiodynamic corrosion analysis. The alloy with 2 at. % Nb instead of Ni showed the best degree of biocompatibility compared to the other alloys.

✉ F. Dagdelen
   fdagdelen@firat.edu.tr

1 Faculty of Science, Department of Physics, Firat University,
   Elazig, Turkey

2 IT Department, Erbil Polytechnic University, Soran Technical
   College, Erbil, Iraq

3 Department of Physics, College of Science, University
   of Raparin, Sulaimaneyah, Iraq

1 Introduction

Materials that can react to specific external stimuli and adapt to their environment are called smart materials [1], and the most important group of them are memory alloys (SMA). SMAs are materials that can reverse the imposed shape change only by heating and under certain conditions [2]. The atomic arrangement of these alloys gives them characteristics like shape memory effect (SME), pseudoelasticity (PE) as well damping capacity [3]. Nowadays, SMAs are used in wide areas, especially in aerospace [4], robotic [5], and biomedical applications [6–8]. Nearly equiatomic Ni–Ti alloys show excellent corrosion [9] and wear resistance [10, 11]. The proportion of nickel in the matrix is one of the most significant parameters governing the resistance and transmutation temperature of Ti–Ni-based alloys [12, 13]. Ni–Ti-based SMAs, which have the widest commercial applications, can be prepared in triple or quaternary form by adding different elements. It is aimed to improve the physical properties such as thermodynamic parameters, phase transformation temperatures, structural and mechanical properties, and biocompatibility by adding other elements to the alloys. It has been reported that the transformation hysteresis, mechanical, and biocompatibility of Ni–Ti SMAs can be affected by the addition of Ta, V, Fe, Cu, and Nb elements [14–17]. It is known that elements such as Zr, Nb, Sn, Ni, and Ta do not have biological side effects. [18]. Niobium has sustained large notice in the biomedical field to develop new alloys, and therefore, it is considered suitable applications for fabrication of devices and structures for junction displacements. Due to the chemical structure containing the element Nb, alloys like that Ti–Nb and Zr–Nb have proven to advance corrosion resistance and biocompatibility [19, 20]. The supplement of Nb element to Ni–Ti alloy can greatly change the phase

stability system of the alloy and can effectively develop the physical properties of the alloy [21]. On the other hand, zirconium (Zr) is suitable for use as a biomaterial because it has certain characteristics such as high fracture toughness and strength, chemical stability, wear and corrosion resistance, high hardness, low thermal conductivity, and biocompatibility [22]. Similar to steel, Zr is biocompatible, hard, and highly radiopaque [23]; moreover, it has a high passivity against electrolytes, great cracking, and bending resistance. There are many studies on the use of elements such as Ti, Nb, Ta, and Zr as biomaterials that do not have toxic effects in the literature; however, crystal structure analysis, thermochemical analysis parameters, and corrosion behavior of quaternary shape memory alloys Ni–Ti–Nb–Zr provide new information about the possibility of using them as bioapplication materials.

It is aimed to manufacture quaternary Ni–Ti–Nb–Zr alloy with different percentages of Ni and Nb to investigate the effect of substituting Nb instead of Ni. The phase transformation between martensite and austenite was studied by differential scanning calorimetry. The crystal microstructure of the alloys was studied through X-ray diffraction and metallurgical microscope. Also, SEM and EDX were used for scanning the surface and analyzing different phases.

2 Material Method

Highly pure (99.9%) Ni, Ti, Zr, and Nb element powders were blended with the help of a mixer. The chemical compositions and coding of the samples are given in Table 1. Three nominal SMAs were labeled as Ti–10Zr–40Ni (SS1), Ti–10Zr–38Ni–2Nb (SS3), and Ti–10Zr–36Ni–4Nb (SS5) in atomic percentage (at.%). The mixed powders were pressed into disks with a diameter of about 13 mm by pressing under a pressure of 90 MPa. Then, the samples were melted by taking them to the arc melting device under an atmosphere of argon gas. Analyses were performed by differential scanning calorimetry (DSC), with each sample in a completed thermal cycle. DSC analyses of the alloys were carried out with a cooling/heating rate of 20 °C/min. DSC analyses of the alloys were made under argon gas atmosphere. In addition, microstructural analysis measurements of the alloys were made using the (SEM–EDX) device. The prepared alloys

were chemically etched in $(HF + NOH_3 + H_2O - 1:2:5)$ solution for approximately 10–15 s. The crystal structure analyses of the samples were determined with the XRD device at room temperature between 30° and 80°. Finally, to determine the biocompatibility behavior of the samples, electrochemical corrosion analysis was applied in the artificial body fluid (SBF). By choosing the potentiodynamic corrosion method; at this stage, assistance was obtained from the Gamry Interface potentiostat/galvanostat/ZRA device. Corrosion analysis and a few parameters related to it; for example, corrosion resistances were calculated using values such as corrosion potential and corrosion current.

3 Results and Discussion

The DSC graph of the alloys performed at a heating–cooling rate of 20 °C.min^{-1} is shown in Fig. 1. Table 2 lists the phase transformation temperatures (PTTs), and the enthalpy changes ($\Delta H^{M \to A}$ and $\Delta H^{A \to M}$) of the alloys, where A_f, A_s, M_f, and M_s are the temperatures that represent austenite finish (A_f), austenite starting (A_s), martensite finish (M_f), and martensite starting (M_s) temperature. The phase structure of Ni–Ti alloys under low temperatures is called as monoclinic crystalline phase B19′, which is known as the martensite phase, and at high temperatures, the phase structure changes to cubic crystalline phase B2, which is called austenite phase. Replacement of Nb with Ni, generally, reduces the phase transformation temperatures compared to the study conducted by Dagdelen et al. on ternary Ni–Ti–Nb SMA [18]. As a result, it can be said that while the Nb element reduces the PTTs, the Ni element increases these temperatures. The value of PTTs and enthalpy change decreases with increasing Nb element content in Ni–Ti–Zr–Nb alloy.

The XRD patterns of SS1, SS3, and SS5 SMAs obtained at room temperature are shown in Fig. 2. The peaks are indexed according to the literature [2, 24–28]. As a result of XRD analysis, martensite (B19′) and austenite (B2) phase peaks are determined in the alloys. B2 and B19′ phases are detected in all samples. The most intense XRD peak is detected in the SS1 sample, which indicates a triple shape memory alloy. By increasing the ratio of Nb element in the Ni–Ti–Zr-based alloy, the XRD peak density of the β-Nb phase (niobium-rich) increases. Balci et al. stated in their study that when the Nb element was added to the Ni–Ti

Table 1 Sample codes and their compositions

	Atomic percentage (at.%)				Weight percentage (wt.%)			
	Ti	Ni	Zr	Nb	Ti	Ni	Zr	Nb
SS1	50	40	10	0	40.0	29.5	30.5	0.0
SS3	50	38	10	2	39.6	27.2	30.2	3.1
SS5	50	36	10	4	39.1	25.0	29.8	6.1
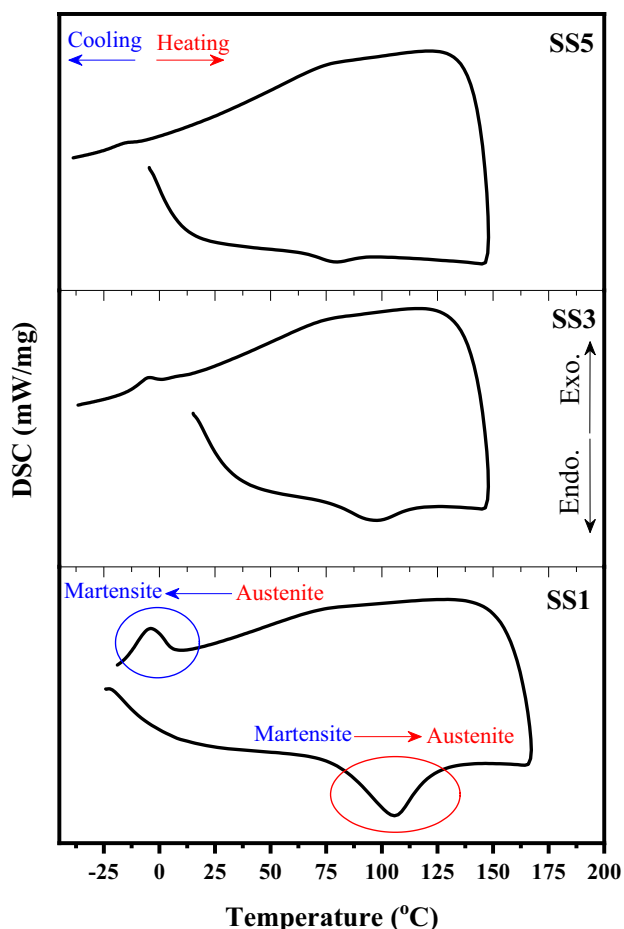
Fig. 1 DSC graph of SS1, SS3, and SS5 SMAs taken at 20 °C.min⁻¹ heating–cooling rate

Fig. 2 XRD pattern of SS1, SS3, and SS5

binary shape memory alloy, they obtained a similar XRD analysis in the case of the β-Nb phase [2].

SEM–EDX analysis and optical microscope (OM) images were taken to examine the microstructural and morphological properties of the alloys. SEM and OM images taken at different magnifications are given in Fig. 3. EDX results obtained for the surfaces of all samples are given in Table 3. As a result, it can be said that the Ti element is dominant and the component participation rate in the chemical structures of the alloy is different for each microstructure. Although there are sediment grains in the structure, no martensite plates are encountered. EDX results are consistent with the nominal atomic ratios. Optical microscope images taken at
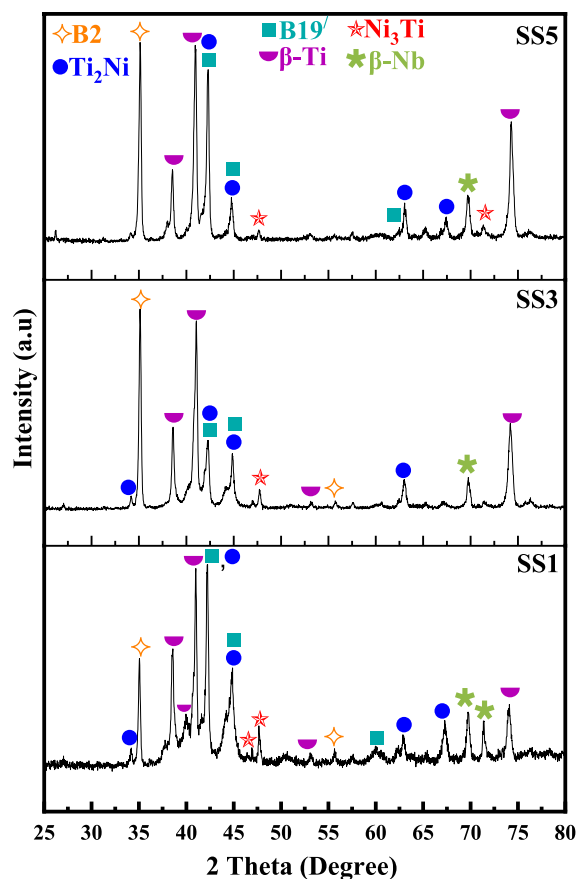
lower magnification than SEM show the presence of dendritic structures and martensitic plates.

In Fig. 4, an SEM image is shown with three spectra obtained for entire surface (Spectrum #10) and two spots (Spectrum #11 and Spectrum #12). The spectra for each cases are illustrated in term of EDS patterns with elemental analysis table. The entire surface of the SS3 sample is nearly the same as the nominal concentration. The other microstructures have Zr and Nb with different concentrations. The high ratio of Ti and Ni shows that second phases could be rare in the alloys. In the microstructures appearing on the surface, both Zr and Nb are dissolved and do not form precipitations or compounds.

The corrosion analysis applied to the materials plays a very important role in the evaluation of these species to be used for biomaterial purposes. Electrochemical methods

Table 2 Phase transformation temperatures and enthalpy changes of alloys at 20 °C.min⁻¹ heating–cooling speed

Sample	A_s (℃)	A_f (℃)	A_p (℃)	M_s (℃)	M_f (℃)	$\Delta H^{M \to A}$ (J/g)	$\Delta H^{A \to M}$ (J/g)
SS1	78.5	122.7	105.7	8.2	−16.3	9.20	−5.86
SS3	76.4	115.5	96.2	3.0	−12.8	3.01	−1.32
SS5	62.5	91.9	78.3	-5.7	−24.2	1.29	−0.45

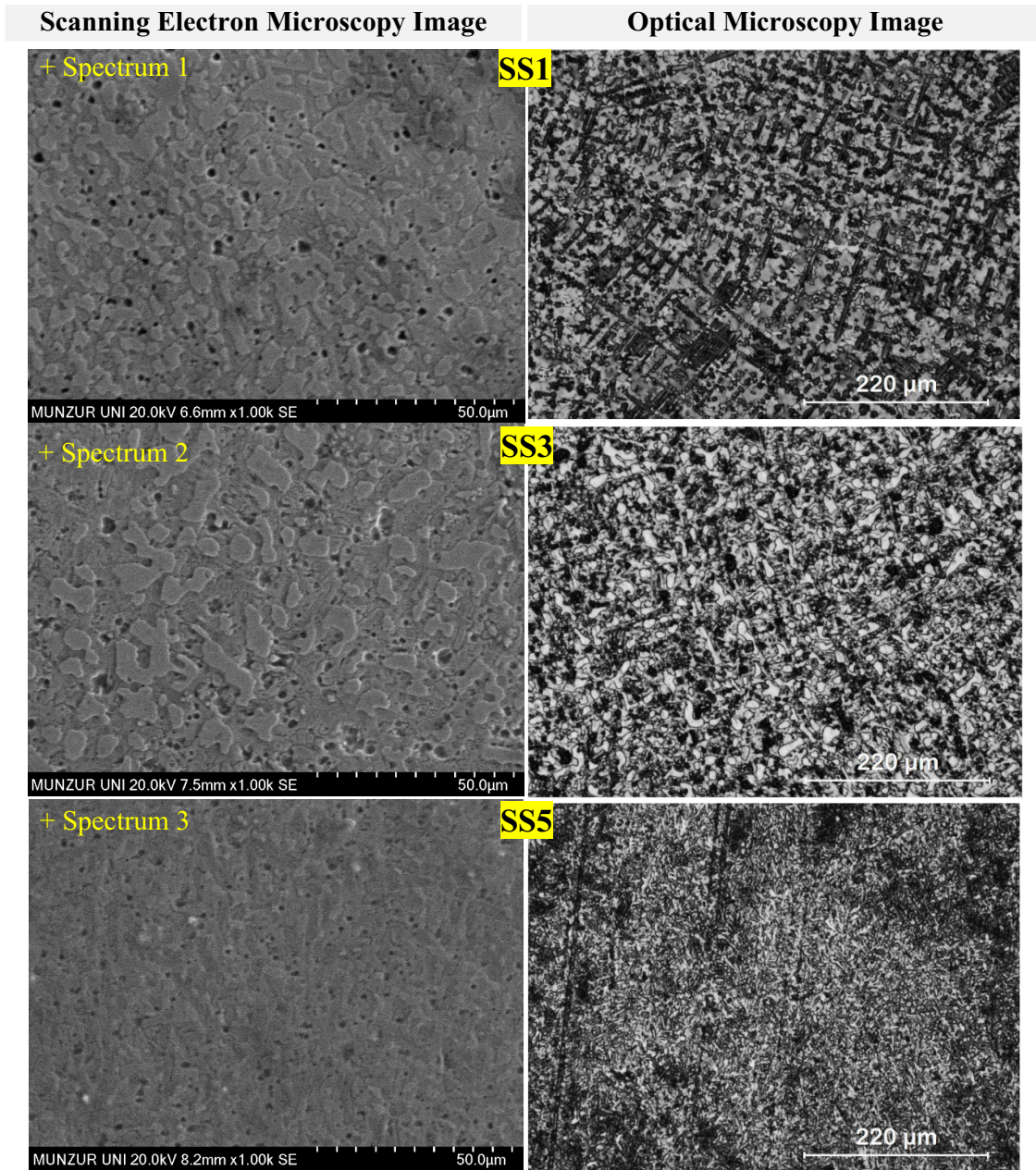| Scanning Electron Microscopy Image	Optical Microscopy Image

Fig. 3 SEM and OM images of SS1, SS3, and SS5

Table 3 SEM images of SS1, SS3, and SS5 SMAs and EDX results from specific regions

Alloy codes	Spectrum no	Constituents (at. %)			
		Ti	Ni	Zr	Nb
SS1	1	49.22	40.85	9.93	–
SS3	2	50.86	36.81	10.24	2.09
SS5	3	50.80	34.54	9.80	4.86

are the most commonly used corrosion analysis by biomaterial researchers. Potentiodynamic measurement, which is one of the electrochemical methods, was carried out for the prepared alloys to examine the corrosion resistance of the alloys. Tafel curves of these measurements made at room temperature are given in Fig. 5. The E_{corr} and I_{corr} parameters obtained as a result of the analyses were obtained by the intersection of the tangential cathodic and anodic lines. Also, the C_R (corrosion rate) was calculated for one-year estimate using the following equation [29]:
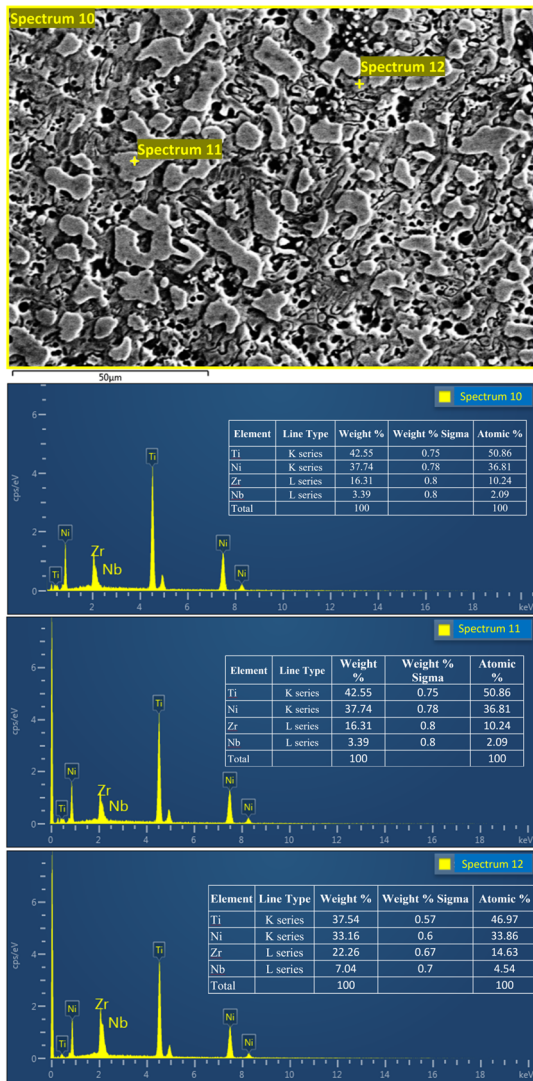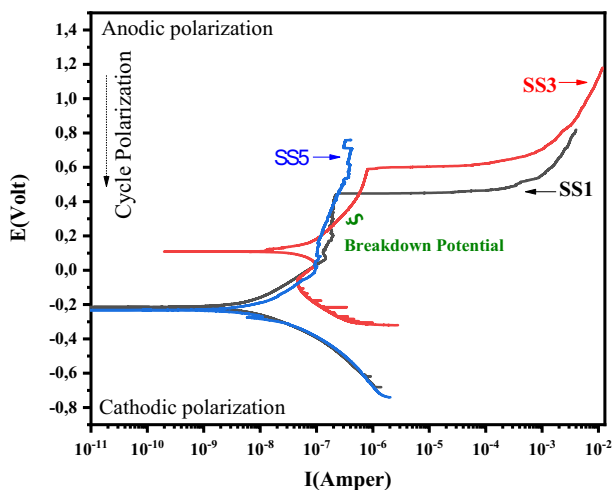
Fig. 4 EDS pattern for three spectra on SS3

Fig. 5 Tafel curve of alloys obtained at room temperature

$$\text{Corrosion rate} = \frac{0.13 \times I_{corr} \times A}{n \times D} \qquad (1)$$

where A is the atomic weight of the constituents, n denotes the number of transferred electrons per s single atom, and D is the density. Table 4 lists the calculated corrosion rate and other related parameters extracted from Tafel curves for all samples. It can be observed that the corrosion of the alloys decreases with the reduction of the corrosion current density (I_{corr}). Here, the lowest corrosion current density belongs to the SS3 sample and it has been determined as the alloy with the highest corrosion resistance. Dağdelen et al. found that the corrosion resistance of the Ni–Ti–Nb alloy reduced with the decline of the Nb element rate [26]. It can be concluded that the current density in SS1 and SS5 alloys increases with the changes of Nb and Ni elements in the SMAs, and also the corrosion resistance value has decreased relatively less and as a result, the degree of biocompatibility has decreased.

4 Conclusions

Assessment of biocompatibility and physical properties of ternary Ti–Ni–Nb and quaternary Ti–Ni–Nb–Zr SMAs were investigated for a diverse amount of Nb and Ni constituents. Some important evaluations obtained as a result of this study are as follows:

- All the samples exhibited austenite (B2) ↔ martensite (B19') phase transformation, which indicated shape memory behavior of all alloys.
- Based on the DSC results, increasing the Nb instead of Ni reduced the phase transformation temperatures of the alloys.
- B2, B19', β-Ti, and some precipitate phases (Ti_2Ni, Ni_3Ti) were detected from XRD results. In addition, by adding Nb element to the alloy, the β-Nb phase was observed in the XRD pattern.
- From the SEM–EDX analysis, it was found that although there were precipitate grains in the structure, no martensite plates were observed; however, the presence of dendritic structures and martensite plates was detected in the optical microscope images.
- The potentiodynamic corrosion test of the alloys taken at room temperature revealed that the sample with the highest degree of biocompatibility was the Ti–10Zr–38Ni–2Nb (SS3) SMA.

Table 4 Electrochemical polarization parameters of alloys at RT

Sample	E_{corr} (V)	β_a (V)	β_c (V)	I_{corr} (µA/cm²)	Corrosion rate (mmpy)	Corrosion resistance (Rp)/ MΩ cm⁻²
SS1	− 213	222.7	160.8	772.0	2.10×10^{-4}	0,052
SS3	− 111	659.1	417.3	161.0	2.15×10^{-4}	0,689
SS5	− 236	202.8	131.5	797.0	2.20×10^{-4}	0,043

Declarations

References

1. Qader I N, Kök M, Dağdelen F and Aydogdu Y, *El-Cezerî Journal of Science and Engineering* **6** (2019) 755.
2. Balcı E and Dagdelen F, *Iranian Journal of Science and Technology, Transactions A: Science* **46** (2022) 353.
3. Ercan E, Dağdelen F, Mediha K and Balci E, *Bitlis Eren Üniversitesi Fen Bilimleri Dergisi* **8** (2019) 1194.
4. Kalra S, Bhattacharya B and Munjal B, *SmMaS* **26** (2017) 095015.
5. Rodrigue H, Wang W, Han M-W, Kim T J and Ahn S-H, *Soft robotics* **4** (2017) 3.
6. Jhou W-T, Wang C, Ii S, Chiang H-S and Hsueh C-H, *J Alloy Compd* **738** (2018) 336.
7. Wen C, Yu X, Zeng W, Zhao S, Wang L, Wan G, Huang S, Grover H and Chen Z, *AIMS Materials Science* **5** (2018) 559.
8. Balci E, Karaderi C C, Kahraman H and Dağdelen F, *International Journal of Innovative Engineering Applications* **6** (2022) 59.
9. Oshida Y and Miyazaki S, *Zairyo-to-Kankyo* **40** (1991) 834.
10. Li D, *Scripta Mater.* **34** (1996) 195.
11. Lin H, He J, Chen K, Liao H and Lin K, *Metallurgical and Materials Transactions A* **28** (1997) 1871.
12. Frenzel J, George E P, Dlouhy A, Somsen C, Wagner M-X and Eggeler G, *Acta Mater* **58** (2010) 3444.
13. Kanca M S, Kök M and Qader I N, *J. Therm. Anal. Calorim.* **147** (2022) 1.
14. Zhang Y-q, Jiang S-y, Zhao Y-n and Tang M, *Transactions of Nonferrous Metals Society of China* **22** (2012) 2685.
15. Mousavi T, Karimzadeh F and Abbasi M, *Materials Science and Engineering: A* **487** (2008) 46.
16. Ying C, Hai-Chang J, Li-Jian R, Li X and Xin-Qing Z, *Intermetallics* **19** (2011) 217.
17. Hamilton R F, Lanba A, Ozbulut O E and Tittmann B R, *Shape Memory and Superelasticity* **1** (2015) 117.
18. Dagdelen F, Balci E, Qader I, Ozen E, Kok M, Kanca M, Abdullah S and Mohammed S, *JOM* **72** (2020) 1664.
19. Dalstra M, Denes G and Melsen B, *Clinical orthodontics and research* **3** (2000) 6.
20. Xu J, Weng X-J, Wang X, Huang J-Z, Zhang C, Muhammad H, Ma X and Liao Q-D, *PloS one* **8** (2013) e79289.
21. Dagdelen F and Aydogdu Y, *J. Therm. Anal. Calorim.* **136** (2019) 637.
22. Hua N, Huang L, Wang J, Cao Y, He W, Pang S and Zhang T, *J. Non·Cryst. Solids* **358** (2012) 1599.
23. Black J, Biological performance of materials: fundamentals of biocompatibility, Crc Press, 2005
24. Li B, Rong L and Li Y, *Science in China Series E: Technological Sciences* **42** (1999) 94.
25. Balci E, Dagdelen F, Qader I N and Kok M, *The European Physical Journal Plus* **136** (2021) 1.
26. Dagdelen F, Balci E, Qader I, Aydogdu Y and Saydam S, *Physics of Metals and Metallography* **122** (2021) 1572.
27. Mitwally M E and Farag M, *Materials Science and Engineering: A* **519** (2009) 155.
28. Sun G, Wang X, Wang Y, Woo W, Wang H, Liu X, Chen B, Fu Y Q, Sheng L and Ren Y, *Materials Science and Engineering: A* **560** (2013) 458.
29. Shahzad K, Sliem M H, Shakoor R A, Radwan A B, Kahraman R, Umer M A, Manzoor U and Abdullah A M, *Sci. Rep.* **10** (2020) 4314.